Journal of Membrane Science 682 (2023) 121787

Contents lists available at ScienceDirect

Journal of Membrane Science

journal homepage: www.elsevier.com/locate/memsci

Tröger's base-regulated interfacial polymerization of polyamide nanofiltration membranes with enhanced performance

Shuqi Liu [a], Zhenggong Wang [a,b,**], Lu Zhao [a], Wangxi Fang [c], Feng Zhang [a,*], Jian Jin [a]

[a] College of Chemistry, Chemical Engineering and Materials Science, Collaborative Innovation Center of Suzhou Nano Science and Technology, Suzhou Key Laboratory of Macromolecular Design and Precision Synthesis, Jiangsu Key Laboratory of Advanced Negative Carbon Technologies, Soochow University, Suzhou, 215123, China
[b] Xinjiang Zhongtai Chemical Co., Ltd., Urumqi, 830000, China
[c] i-Lab, Suzhou Institute of Nano-Tech and Nano-Bionics, Chinese Academy of Sciences, Suzhou, 215123, China

ARTICLE INFO

Keywords:
Nanofiltration membrane
Polyamide layer
Interfacial polymerization
Tröger's base
High permeability

ABSTRACT

Interfacially fabricated polyamide thin film composite (TFC) membranes have been widely used in molecular and ion nanofiltration. However, it is still a great challenge to desirably control the thickness and performance of polyamide layer due to the uncontrollable interfacial polymerization (IP) process. In this work, Tröger's base (TB), consisting of two benzene rings connected by a bicyclic aliphatic methanodiazocine unit was used to regulate the IP between trimesoyl chloride (TMC) and piperazine (PIP). The incorporation of TB molecule accelerates the diffusion rate of PIP toward the water/hexane interface and enhances the reaction activity of TMC as a catalyst, thus largely promoting the interfacial reaction rate and resulting in the formation of polyamide layer with an extremely thin thickness. The thickness of the polyamide layer was tuned from 63.1 to 17.4 nm by increasing the TB content in aqueous solution. The TFC nanofiltration membrane fabricated through TB regulated IP process showed a water permeance of 18.5 ± 1.4 L m^{-2} h^{-1} bar^{-1} and simultaneously a salt rejection of 98.3% for Na_2SO_4 with overall desalination performance exceeding most nanofiltration membranes and commercial membranes. This work proposes a strategy for regulating the reaction rate of PIP and TMC during the IP process using a TB structured additive, which provides an alternative means for fabricating highly permeable TFC nanofiltration membranes.

1. Introduction

Rational utilization and protection of water resources is a long-term, important, and arduous task [1,2]. Compared with traditional separation processes, membrane separation technology has good prospects in efficiently accessing drinking water from urban sewage, groundwater, seawater, *etc.* [3,4]. Nanofiltration (NF) is a membrane separation technology that enables a low molecular weight cut-off (MWCO) of 200–1000 Da in the aperture range of 0.5–2 nm [5,6]. This unique property makes NF suitable for desalination, drinking water softening, and removal of pollutants and heavy metal ions from wastewater [7–10]. Polyamide prepared by interfacial polymerization (IP) is the most widely applied NF membrane material owing to its high separation efficiency and ease of scaling up [11]. Although the cross-linked structure of selective layer could achieve high rejection, it would also result in low water flux, restricting further development of nanofiltration technology.

Extensive efforts have been dedicated to regulate the molecular structure and macrostructure of polyamide nanofilm to improve the permselective performance of TFC NF membranes [12–15]. Among them, decreasing membrane thickness is the most direct and effective strategy to decrease mass transfer resistance and increase membrane flux. The interlayer strategy for fabrication of an ultrathin selective layer was first proposed by Livingston's group and further developed by many other researchers [16]. Organic materials including dopamine [17], chitosan [18], tannic acid (TA)/Fe^{3+} [19], as well as inorganic materials, including carbon nanotubes (CNTs) [20], cellulose nanocrystals (CNCs) [21], MXenes [22], covalent organic frameworks (COFs) [23]

* Corresponding author.
** Corresponding author. College of Chemistry, Chemical Engineering and Materials Science, Collaborative Innovation Center of Suzhou Nano Science and Technology, Suzhou Key Laboratory of Macromolecular Design and Precision Synthesis, Jiangsu Key Laboratory of Advanced Negative Carbon Technologies, Soochow University, Suzhou, 215123, China.
E-mail addresses: zgwang2017@suda.edu.cn (Z. Wang), fzhang2018@suda.edu.cn (F. Zhang).

https://doi.org/10.1016/j.memsci.2023.121787
Received 23 February 2023; Received in revised form 13 May 2023; Accepted 28 May 2023
Available online 29 May 2023

and metal organic frameworks (MOFs) [24] have been used as an interlayer to adjust the pore size and surface structure of the selective layer. However, the relatively large surface pores of the inorganic nanomaterials interlayer tend to cause local defects under high pressure, resulting in a certain degree of loss to the solute rejection. In addition, the process of preparing such a three-layer structure NF membrane is complex, and the choice of materials is limited due to the pore size required for the interlayer.

Adding additives is another commonly used method to effectively adjust the polymer structure and the thickness of the polyamide nanofilm by regulating the IP process. Generally, the decrement of the thickness of the polyamide layer is achieved by the addition of additives such as glycerin [12], phytic acid dodecasodium salt (PADS) [25], poly (vinyl alcohol) (PVA) [26], *etc.* into aqueous solution to reduce the diffusion rate of piperazine (PIP) through hydrogen bond interaction or electrostatic interaction in the IP process. Although the thickness of the polyamide layer is reduced by decreasing the diffusion rate of PIP, and the water permeance of the membrane is increased as well. This approach often leads to a decrease in the cross-linking degree of the polyamide layer thus resulting in a decrease of the solute rejection [27,28]. Nevertheless, reducing the thickness of selective layer can also be implemented by promoting the monomer's transfer and accelerating the interfacial reaction rate [29,30]. The fast monomer enrichment at the interface can trigger the rapid formation of a highly cross-linked dense primary layer and inhibit the further accumulation of the thickness of the selective layer. From this point of view, this method could not only reduce the thickness of the selective layer but also ensure the cross-linking degree of the selective layer due to intensified IP reaction with high-density monomer in the interface. However, up to now, few additives have been explored to regulate the IP reaction by promoting the monomer diffusion.

Tröger's base (TB), first proposed by Tröger in 1887 is constructed by two benzene rings connected by a bicyclic aliphatic methanodiazocine structure. This unique structure endows TB with a rigid V-shaped configuration and a hydrophobic cavity [31,32]. Therefore, the two tertiary amine N atoms in TB are exposed to the reactants and act as active sites to catalyze the reaction [33,34]. The fixed configuration of TB renders it useful in molecular recognition, catalysis, bioorganic and supramolecular chemistry [35,36]. Herein, we proposed a Tröger's base regulated IP process between PIP and trimesoyl chloride (TMC) for the fabrication of polyamide TFC NF membrane (Fig. 1a). Small amount of TB was added in the PIP aqueous solution and regulated the IP reaction in two ways. On the one hand, TB acts as a catalyst to enhance the activity of TMC [15,37]. On the other hand, the TB moiety interacts with PIP *via* strong hydrogen bond to accelerate the diffusion rate of PIP toward the water/hexane interface, as shown in Fig. 1b. The addition of TB effectively promotes the interfacial reaction rate and achieves the formation of a polyamide nanofilm with extremely thin thickness. The thickness of polyamide layer fabricated *via* the TB regulated IP process is as thin as 17.4 nm. The corresponding TFC NF membrane shows a water permeance of 18.5 ± 1.4 L m^{-2} h^{-1} bar^{-1} almost two-folds higher than those of the membranes prepared from the common IP process without addition of additives and simultaneously a high Na_2SO_4 rejection up to 98.3%.

2. Experimental

2.1. Materials

Polyethersulfone (PES) ultrafiltration membrane (MWCO 50000 Da) was purchased from Microdyn-Nadir Co. Ltd. (Germany). Tröger's base (2,8-dimethyl-6H,12H-511-methanodibenzo [b,f] [1,5] diazocine) was purchased from Sigma-Aldrich. Trimesoyl chloride (TMC, >98%) was purchased from J&K Scientific (Shanghai, China). Piperazine (PIP, >99.0%), sodium sulfate (Na_2SO_4, ≥99%), magnesium sulfate ($MgSO_4$, ≥98%), sodium chloride (NaCl, ≥99.5%), alizarin red (AR, 99%) were purchased from Sigma-Aldrich. Hexane, ethanol, methanol, N, N-dimethylformamide (DMF) were purchased from Chinasun Specialty Products Co., Ltd. (China).

2.2. Preparation of TFC NF membranes

First, the aqueous solution with and without TB added were all dissolved in the water containing 10% ethanol (v/v%) by sonication, followed by heating in a water bath until a homogeneous solution was formed. Then PES substrate membrane was first immersed in PIP solutions (with different TB concentrations) for 2 min, and then the membrane was taken out. The excess solution is drained off from the surface. Then the wet membrane was totally immersed in 1.5 mg mL^{-1} TMC hexane solution for another 30 s to perform the IP reaction. The obtained

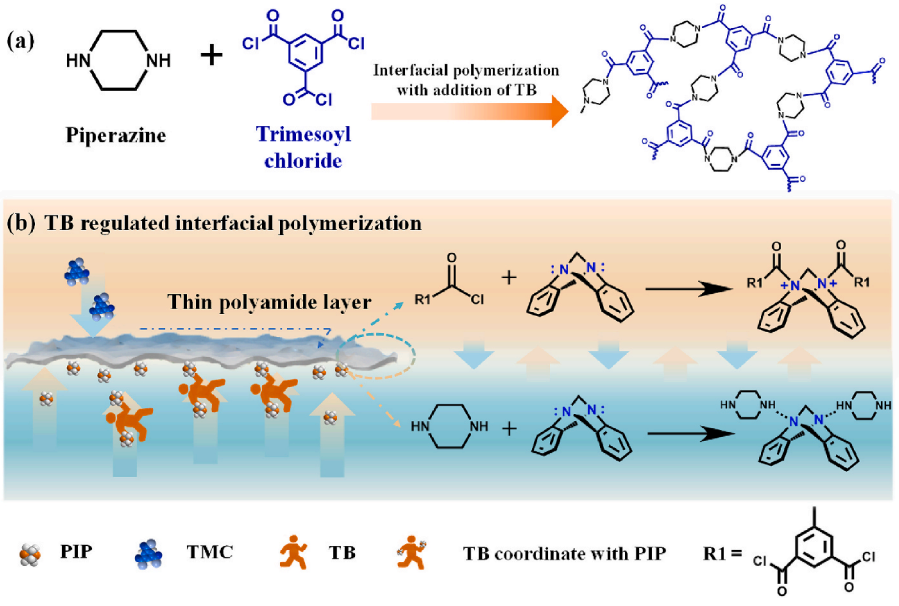

Fig. 1. Schematic illustration of the fabrication of polyamide layer *via* TB regulated IP (a) Chemical reaction between TMC and PIP; (b) Mechanism of TB regulated IP.

membrane was washed using hexane and then heated at 60 °C for several minutes. The obtained membrane was stored in pure water for further use.

The PIP concentration of the aqueous solution was fixed at 4.0 mg mL^{-1}, and the molar ratio of TB with PIP was shown in Table 1. The as-prepared TFC NF membranes were denoted as M-TB_x-P_y, where x and y represent the molar ratio of TB and PIP. The membrane of M-P was prepared by only 4.0 mg mL^{-1} PIP. The membrane M-TB_1-P_{20} was obtained from the aqueous solution containing TB and PIP (4.0 mg mL^{-1}), whose molar ratio was 1:20, and other membranes were named in the same way.

2.3. Membrane characterization

Fourier transform infrared spectroscopy (FTIR, IRTracer-100) and X-ray photoelectron spectroscopy (XPS, EXCALAB 250 XI) were used to detect the TFC membrane surface property. The morphology of the TFC membrane was observed by field emission scanning electron microscope (FE-SEM, Hitachi S-8230). The PA nanofilm thickness was measured by an atomic force microscope (AFM, Dimension Icon, Bruker) [38,39] (see supplementary material for details). The water contact angle (WCA) of the TFC membranes were evaluated by dropping 3 μL of pure water using OCA20 (Data-physics) to test the membrane wettability. The zeta potential of the TFC membrane was characterized by an electrokinetic analyzer (Sur-PASS 3, Anton Paar, GmbH). The PIP diffusion was monitored using ultraviolet–visible (UV–vis) spectroscopy (Hitach Co, UV-2700) and gas chromatograph (Agilent 7820 GC).

The separation performances of TFC NF membranes were evaluated by a cross-flow filtration device. The effective test area of each membrane was 7.1 cm^2. The cross-flow rate was 0.2 m s^{-1} and the applied pressure was 2 bar. The testing solutions of salts were 1000 ppm and the salt rejection was obtained through a conductivity meter (METTLER TOLEDO S230).

The pore size distribution of the as-prepared TFC NF membranes were calculated by the rejection of a series of neutral organic compounds with increased molecular weight. The neural organic compounds tested in this study include glycerol (92 Da), glucose (180 Da), sucrose (342 Da) and raffinose (504 Da). The concentration of each organic species solution was 200 ppm, and the applied pressure in the filtration experiments was 2 bar. The MWCO of TFC NF membrane was defined as the molecular weight at which the rejection equals 90%. The pore size distribution curve is expressed as a probability density function (PDF) that was established based on the following assumption: (1) There is no steric or hydrodynamic interaction between these organic solutes and the membrane pores; (2) The mean pore size of the polyamide membrane equals the Stokes radius of the organic solute with a measured rejection of 50%; (3) The distribution of the membrane pore size is characterized by the geometric deviation of the PDF curve, which is the ratio between the Stokes radius with a rejection of 84.13% to that with a rejection of 50% [40,41]. The pore size distribution function is the following Eq. (1):

$$\frac{dR(r_p)}{dr_p} = \frac{1}{r_p \ln \sigma_p \sqrt{2\pi}} \exp\left[-\frac{(\ln r_p - \ln \mu_p)^2}{2(\ln \sigma_p)^2} \right] \quad (1)$$

Table 1
Molar ratio of TB to PIP in various M-TB_x-P_y membranes.

Membranes	n(TB):n(PIP)
M-P	–
M-TB_1-P_{40}	1:40
M-TB_1-P_{20}	1:20
M-TB_1-P_{10}	1:10
M-TB_1-P_5	1:5

where μ_p is the mean pore size, σ_p is the geometric standard deviation of the PDF curve and r_p is the Stokes radius of the organic solute. The Stokes radius of these molecules correlate with their molecular weight by Eq. (2):

$$\log(r_p) = -1.4962 + 0.4654 \log(M_w) \quad (2)$$

where M_W is the molecular weight of each organic solute. Based on the above equation, the Stokes radius for glycerol, glucose, sucrose, and raffinose are 0.184, 0.251, 0.338, and 0.405 nm, respectively.

3. Results and discussion

3.1. Characterization of as-prepared TFC NF membranes

Fig. 2a shows the FTIR spectra of TFC NF membranes prepared with different molar ratio of TB and PIP in the aqueous phase. The new absorption peaks at 1455 cm^{-1} and 1630 cm^{-1} are correlated to the C=O stretching vibration (amide I) in the formed amide groups, and the peak at 1581 cm^{-1} was due to the C–N stretching vibration (amide II) of the amide bond [25,42]. Fig. 2b shows the WCA of the membrane surface, as the molar ratio of n(TB):n(PIP) in the aqueous phase increased from 0 to 1:5, the WCA of the membrane gradually increased from 38.7° to a maximum of 64.5°. The chemical composition of the polyamide nanofilm was analyzed by XPS. The four peaks in the C1s spectrum are assigned to O=C–O, O=C–N, C–N and C–C in the polyamide layer, respectively (Figs. S1–S2). The O=C–N group is derived from the reaction of the acyl chloride in TMC monomers with the secondary amines in the PIP monomer. The O=C–O group is mainly derived from the carboxyl acid group formed by the hydrolysis of the unreacted acyl chloride group. The cross-linking degree of the as-prepared membranes were calculated according to the O/N element ratio in the XPS spectrum (Table S1). The cross-linking degree of the polyamide layer for the M-P membrane is 73.1% and gradually increases when increasing the TB content. The highest cross-linking degree of 84.7% is obtained for the M-TB_1-P_5 with the highest TB content. It is hypothesized that the addition of TB in an aqueous phase can promote the polymerization reaction thus leading to the increment on the cross-linking degree of the polyamide nanofilm. The gradual increment of cross-linking degree led to the progressive increase of WCA of the polyamide layer, as illustrated in Fig. 2c. In Fig. 2d, zeta potential characterization shows that the membranes possess similar surface charges with isoelectric points (IEPs) in a close range of pH = 3.9–4.4. Due to the presence of carboxylic acid functional groups in the polyamide layer, all the membranes are negatively charged above the IEPs.

Fig. 3 shows the thickness variation of the polyamide nanofilm with different TB contents in PIP aqueous solution. The vertical drop between the nanofilm and silicon was regarded as the thickness of the nanofilms and characterized by atomic force microscope. As shown in Fig. 3a, the polyamide nanofilm on the M-P membrane shows a thickness of 63.1 nm while the thickness decreases to 41.3 nm with a small amount of TB addition (n(TB):n(PIP) = 1:40). Increasing the molar ratio of TB to PIP leads to thinner polyamide nanofilms. The thinnest polyamide nanofilm with a thickness of 17.4 nm was achieved by M-TB_1-P_5. It is indicated that the TB introduction brings about decrement on the thickness of the polyamide nanofilm, and the thickness can be well manipulated by tuning the molar ratio of TB and PIP in aqueous solution, as summarized in Fig. 3f. As a controlled experiment, triethylamine (TEA) with a similar tertiary amine structure, which is often used to promote the IP reaction between diamine and acyl chloride, was added into the PIP aqueous solution to investigate the polyamide nanofilm thickness variation. The results indicate that the polyamide nanofilm thickness and the pure water permeance are not changed significantly with TEA addition (Figs. S3–S4).

As we know, the thickness of the polyamide nanofilm is generally manipulated by controlling the diffusion rate of the monomers in

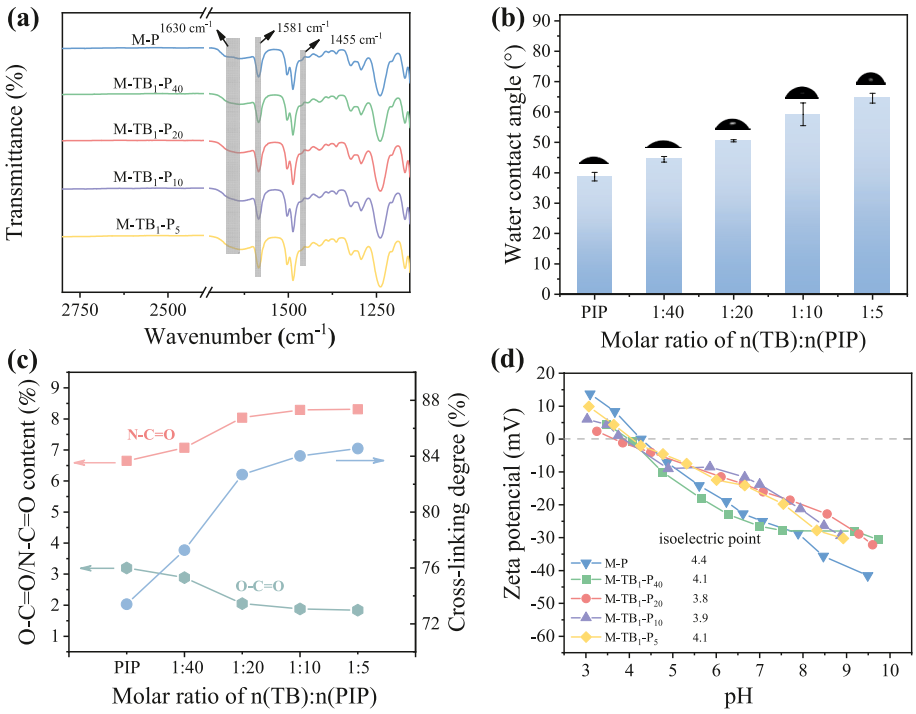

Fig. 2. Surface properties of as-prepared TFC NF membranes. (a) FTIR spectra and (b) WCA of the membrane with different TB contents; (c) Content of O=C–N, O=C–O and cross-linking degree of the polyamide layers; (d) Zeta potential.

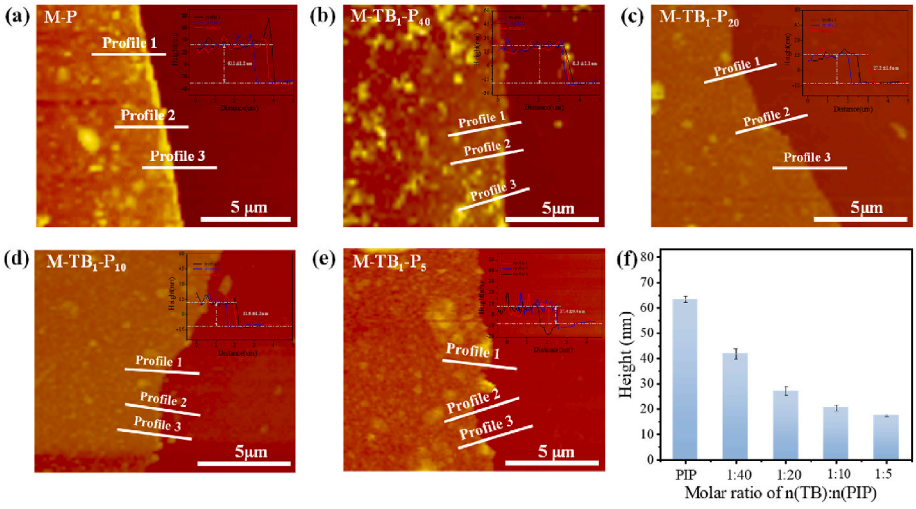

Fig. 3. (a–e) AFM images and (f) Summary of the height profiles of the polyamide nanofilms fabricated from PIP aqueous solutions with different TB contents.

aqueous phase to the aqueous/organic interface. The diffusion behavior of PIP in an aqueous solution with different contents of TB was monitored *via* the previously reported method using a UV–vis spectrometer, as schematically illustrated in Fig. S5 [12]. As the secondary amine groups of PIP can react with the quinone groups of AR to form a charge-transfer complex, the diffusion and consumption of PIP in the IP process was observed from the change of absorption intensity of the complex. The UV–vis spectra in Fig. S6 show that the complex has an absorption peak at 517 nm, and the peak intensity displays a linear relationship with the PIP concentration in the aqueous phase. Fig. 4a demonstrates a real-time change in PIP concentration near the aqueous/organic interface. The higher ratio of the TB in the aqueous solution, the lower the absorption intensity of the complex in the UV-spectrum under the same polymerization time.

We also used GC to detect the diffusion rate of PIP with different TB contents in aqueous solution *via* detecting the PIP concentration near the aqueous/organic interface in hexane (Fig. S7). The concentration of PIP in hexane with the same diffusion time was determined by the peak area of PIP in GC and calculated according to the standard curve (Fig. S8), the results are shown in Fig. 4b. The concentration of PIP without TB addition was ~7.9 ppm and then increased to ~22.3 ppm with TB addition with a molar ratio between TB and PIP of 1:40, which was two times higher than that of the solution without TB. Further increasing the TB content leads to a higher PIP concentration, and the highest PIP concentration of ~123.9 ppm was observed in hexane when the molar ratio between TB and PIP was 1:5. These results clearly indicate that the diffusion of PIP is promoted by increasing the molar ratio of TB, which in turn regulates the IP process and the thickness of the polyamide nanofilms. On the one hand, TB with a benzene ring structure is more oleophilic and more conducive to diffuse to the organic phase. On the other

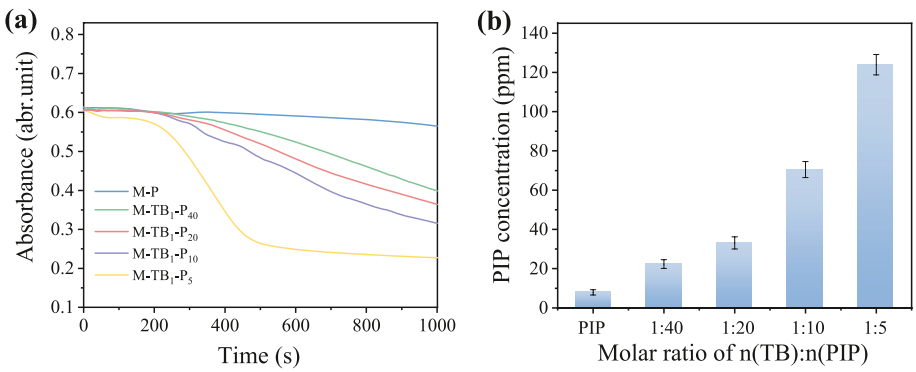

Fig. 4. (a) UV–vis spectra of the real-time change in PIP concentration near the aqueous/organic interface; (b) PIP concentration in the organic phase after 60 s diffusion measured by GC.

hand, the TB moieties can interact with PIP *via* strong hydrogen bonds, thus accelerating the diffusion rate of PIP toward the water/hexane interface which has been shown in Fig. 1b. Besides, the TB can also catalyze the reaction between PIP and TMC and the possible mechanism is shown in Fig. S9. The rapidly formed primary layer prevents further diffusion of the monomer, contributing to the formation of a thinner polyamide nanofilm. In comparison with TEA additive, the twisted structure of TB can fully expose the double-bridged association of N atom, which plays a crucial role in enhancing the reaction efficiency and decrement in the thickness of the polyamide nanofilm.

The surface morphology of the polyamide layer on the TFC NF membrane was analyzed by SEM and the images are presented in Fig. 5. All the membranes show dense and continuous structure without obvious defects observed on the top surface, which is different from the porous structure of the surface of PES support membrane (Fig. S10). The top surface of the polyamide layer of the M-P membrane is smooth using the solution containing only PIP. In comparison, the polyamide layer of M-TB_1-P_{20} shows a much rougher structure with prominent nodules appeared on the top surface. The nodular-like structures are generated from the larger reactive particles due to the enhanced heat convection at the aqueous/organic interface with TB addition [43,44]. The similar morphology was also observed on the top surface of the M-TEA_1-P_5 polyamide layer fabricated from the PIP solution using TEA as the catalyst. Further increasing TB contents in aqueous solution, the nodule-like structures increase and become larger due to further intensified reaction with higher TB content as illustrated in Fig. S11. The surface roughness of the membranes measured by AFM are in consistent with SEM characterization as shown in Fig. S12. For the morphologies of the bottom surface in Fig. 5d–f, all the polyamide layers show similar dense and smooth structures. These results confirm that the addition of TB can promote the interfacial reaction through a synergetic mechanism of acceleration of PIP diffusion and catalysis of the IP reaction.

We also conducted the experiments to directly observe the effect of TB on the reaction by adding TB in the organic phase, three hexane solutions containing TMC, TMC&TEA, TMC&TB respectively were explored for the experiments, while PIP solution was used as the aqueous phase. The real-time reactions were recorded by video as shown in the supporting information. The optical images of the solution after 30 s IP reaction are shown in Fig. 6a–c. The violent reaction occurred at the interface using TMC&TB solution as the organic phase. As a result, no nanofilm is observed at the interface, but white precipitates were observed in hexane which is different from the other two solutions, where the nanofilm can be obtained for the organic solutions containing TMC and TMC&TEA, respectively. FTIR characterization in Fig. 6d and e shows that the white products in hexane are oligomers of polyamide. It is assumed that the violent reaction destroys the interface and some PIP monomers at the aqueous/organic interface are captured to the hexane by TB and form PA oligomers in the hexane. These results demonstrate the strong interaction between PIP and TB and the catalytic performance of TB. The addition of TEA shows less effect on the reaction due to its fewer active sites in comparison with TB.

3.2. MWCO, pore size distribution and separation performance of the as-prepared TFC NF membranes

As shown in Fig. 7a and b, the MWCO value slightly decreases from 403 Da to 356 Da as the molar ratio of TB and PIP increases from 0 to 1:5, while the average pore size of the membrane changes from 0.61 nm to 0.58 nm, indicating slightly decrement of pore size in the TFC NF membranes with the addition of TB in aqueous solution. The separation

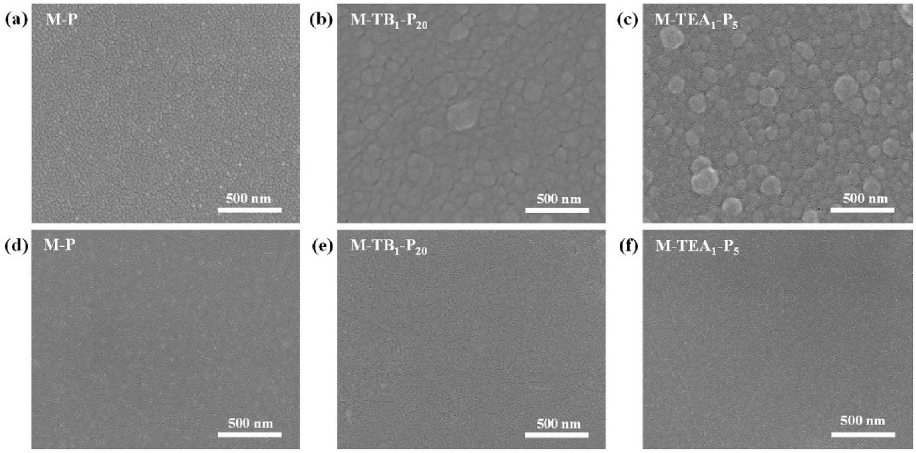

Fig. 5. Morphological characterization of as-prepared TFC NF membranes. (a–c) SEM images of the top surface; (d–f) SEM images of the bottom surface.

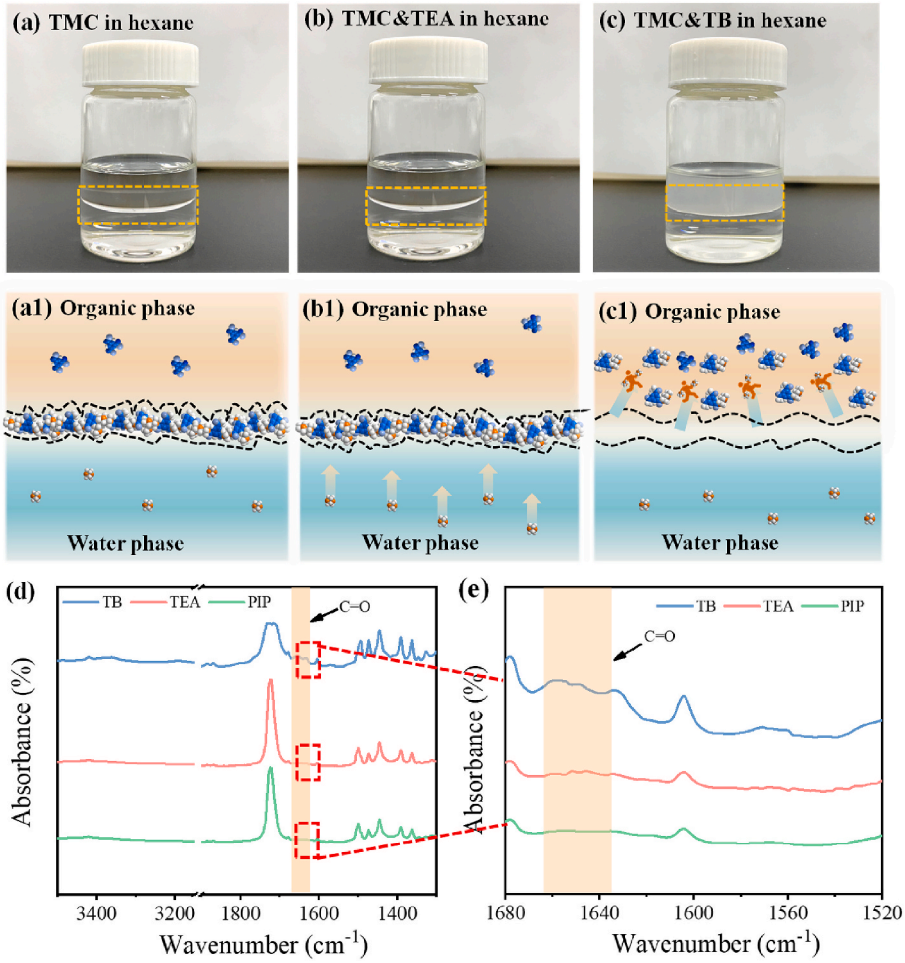

Fig. 6. (a–c) Optical images of the organic phase containing only TMC, TMC&TEA and TMC&TB; (a1-c1) Schematically illustration of molecular microscopic motion during the reaction; (d) FTIR characterization of products in organic phase solution and (e) Enlarged view of FTIR in the range of 1520–1680 cm^{-1}.

performance of the as-prepared TFC NF membranes is shown in Fig. 7c. The water permeance of the M-P membrane without TB in PIP aqueous solution is 8.5 ± 1.6 L m^{-2} h^{-1} bar^{-1}, the water permeance increases with TB addition and achieves 18.5 ± 1.4 L m^{-2} h^{-1} bar^{-1} for the M-TB_1-P_{20} membrane when the molar ratio of TB and PIP in aqueous solution is 1:20, which is two-folds higher than the water permeance of the contrasted M-P membrane. However, further increasing the TB content in PIP aqueous solution leads to the decrement of water permeance, and the M-TB_1-P_5 membrane shows a water permeance of 9.9 ± 1.2 L m^{-2} h^{-1} bar^{-1}. The decrement of water permeance is due to the increased cross-linking degree and also the resulting narrowed pore size of the polyamide nanofilm with high TB content in aqueous solution. As a typical example, the M-TB_1-P_{20} membrane shows the salt rejection values of around 98.3% for Na_2SO_4, 93.9% for $MgSO_4$, 47.3% for $MgCl_2$ and 23.9% for NaCl, which is slightly higher than the salt rejection of the M-P membrane without TB addition (Fig. 7d). In comparison with some commercial and TFC NF membranes reported in the literature, the as-prepared TFC NF membranes fabricated from the TB regulated IP process exhibit a superior balance between water permeance and salts rejection which due to the decreased thickness and proper pore size of the membranes (Table S2 and Fig. S13.).

3.3. The stability of TFC NF membranes

Fig. 8a shows the water fluxes of M-P and M-TB_1-P_{20} under different tested pressures. The water flux of M-TB_1-P_{20} was 35.9 ± 2.8 L m^{-2} h^{-1} compared to M-P (17.8 ± 1.4 L m^{-2} h^{-1}) at 2 bar. Furthermore, the water flux of M-TB_1-P_{20} still remains two-folds higher compared to the TFC NF membrane fabricated without TB addition during the IP process at a higher applied pressure of 5 bar. These results demonstrate that the as-prepared TFC NF membranes show good permeate stability during the separation process even under higher applied pressure. We also evaluated the influence of different concentrations of salt solutions on the membrane separation performance. Fig. 8b shows the water flux of the M-P and M-TB_1-P_{20} membranes at different salt concentrations. The results indicate that the M-TB_1-P_{20} membrane with higher water flux is viable for concentrated salt solutions with concentrations from 1000 ppm to 7000 ppm. Besides, the M-TB_1-P_{20} membrane shows long-term stable water flux and salt rejection value during continuous operation under cross-flow conditions (Fig. S14).

4. Conclusion

In this work, a new type of polyamide TFC NF membrane with reduced thickness and improved water permeance was successfully prepared by TB regulated IP. TB was added in aqueous phase to accelerate the diffusion rate of PIP toward the water/hexane interface and also acted as a catalyst to enhance the reaction activity of TMC, thus forming a thinner selective layer compared with the traditional IP process. The thickness of the polyamide layer is linearly regulated from 63.1 nm to 17.4 nm by simply changing the molar ratio of TB and PIP from 0 to 1:5. The reduction in membrane thickness reduces the mass transfer barrier and improves the water permeance. The TFC NF membrane exhibits high performance with a water permeance of 18.5 ± 1.4

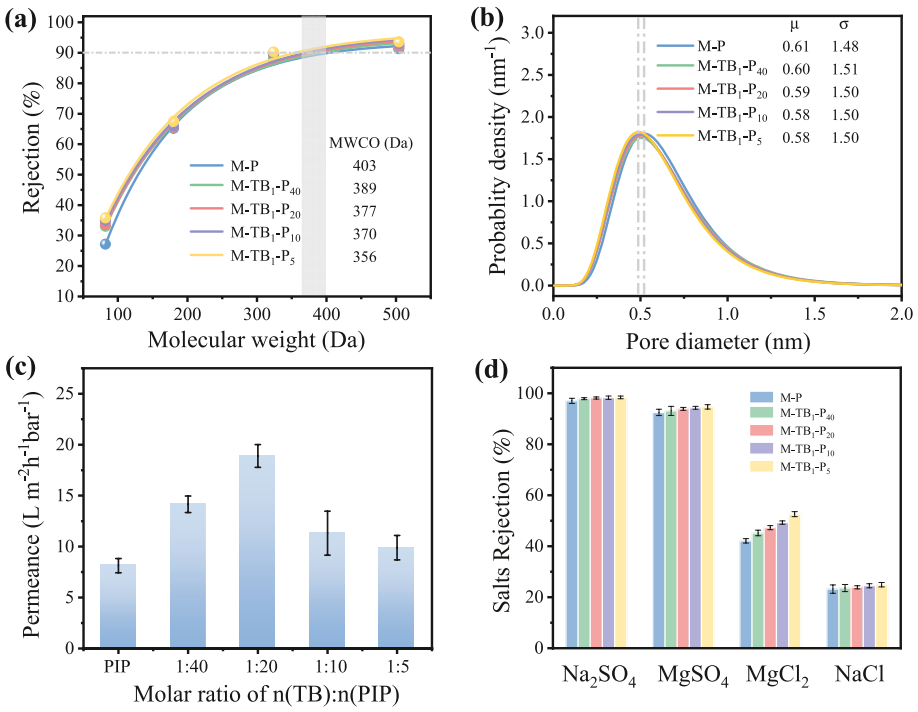

Fig. 7. (a) MWCOs and (b) Pore size distribution of the TFC NF membranes. Separation performance of the as-prepared TFC NF membranes: (c) Water permeance and (d) Salt rejection test using 1000 ppm salts solution at 2 bar.

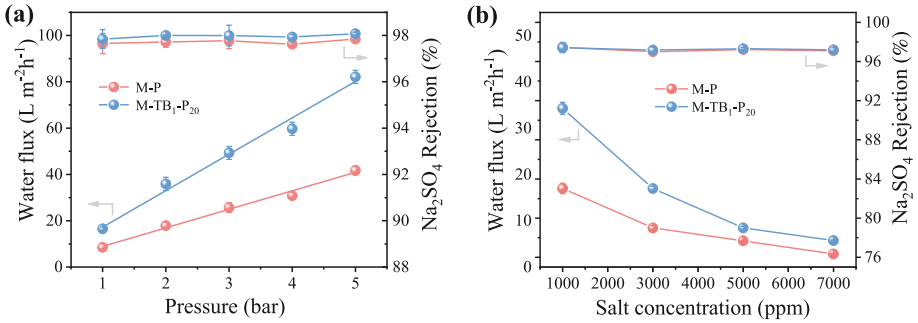

Fig. 8. (a) Water flux and Na_2SO_4 rejection value of the M-P and M-TB_1-P_{20} membranes at different applied pressure; (b) Water flux and Na_2SO_4 rejection of the M-P and M-TB_1-P_{20} membranes at different salt concentrations.

L m^{-2} h^{-1} bar^{-1} and Na_2SO_4 rejection of 98.3%, yielding an overall desalination performance superior to most of reported NF membranes. This work provides a strategy to regulate the reaction rate of PIP and TMC during the IP process and achieves advanced TFC NF membranes with enhanced performance.

Author contributions

Shuqi Liu: Methodology, Investigation, Data Curation, Writing-Original draft preparation, Writing-review & editing. **Zhenggong Wang**: Conceptualization, Formal analysis, Resources. **Lu Zhao**: Formal analysis, Writing-original draft. **Wangxi Fang**: Supervision, Formal analysis. **Feng Zhang**: Formal analysis, Writing-review & editing, Resources, Supervision. **Jian Jin**: Supervision, Writing-review & editing, Project administration.

Declaration of competing interest

The authors declare that they have no known competing financial interests or personal relationships that could have appeared to influence the work reported in this paper.

Data availability

Data will be made available on request.

Acknowledgements

The authors are thankful for the financial support from the National Key Research and Development Plan (Grant No. 2022YFB3805903, 2019YFA0705800), the National Natural Science Foundation of China (Grant No. 21988102), the Key Research and Development Plan of JiangSu Province (BE2022056). The authors also thank the support from Jiangsu Key Laboratory of Advanced Functional Polymer Design and Application, Soochow University.

Appendix A. Supplementary data

Supplementary data to this article can be found online at https://doi.org/10.1016/j.memsci.2023.121787.

References

[1] M.M. Mekonnen, A.Y. Hoekstra, Four billion people facing severe water scarcity, Sci. Adv. 2 (2016), e1500323, https://doi.org/10.1126/sciadv.1500323.

[2] M. Salehi, Global water shortage and potable water safety; Today's concern and tomorrow's crisis, Environ. Int. 158 (2022), 106936, https://doi.org/10.1016/j.envint.2021.106936.

[3] M.A. Shannon, P.W. Bohn, M. Elimelech, J.G. Georgiadis, B.J. Mariñas, A. M. Mayes, Science and technology for water purification in the coming decades, Nature 452 (2008) 301–310, https://doi.org/10.1038/nature06599.

[4] A. Lee, J.W. Elam, S.B. Darling, Membrane materials for water purification: design, development, and application, Environ. Sci.: Water Res. Technol. 2 (2016) 17–42, https://doi.org/10.1039/c5ew00159e.

[5] G.M. Shi, Y. Feng, B. Li, H.M. Tham, J.Y. Lai, T.S. Chung, Recent progress of organic solvent nanofiltration membranes, Prog. Polym. Sci. 123 (2021), 101470, https://doi.org/10.1016/j.progpolymsci.2021.101470.

[6] A.W. Mohammad, Y.H. Teow, W.L. Ang, Y.T. Chung, D.L. Oatley-Radcliffe, N. Hilal, Nanofiltration membranes review: recent advances and future prospects, Desalination 356 (2015) 226–254, https://doi.org/10.1016/j.desal.2014.10.043.

[7] W.H. Yu, Z.Q. Gan, J.R. Wang, Y. Zhao, J. Han, L.F. Fang, X.Z. Wei, Z.L. Qiu, B. K. Zhu, A novel negatively charged nanofiltration membrane with improved and stable rejection of Cr (VI) and phosphate under different pH conditions, J. Membr. Sci. 639 (2021), 119756, https://doi.org/10.1016/j.memsci.2021.119756.

[8] C. Dong, Y. Huang, H. Lin, L. Zhang, Performance intensification and anti-fouling of the two-phase flow enhanced direct contact membrane distillation for seawater desalination, Desalination 541 (2022), 116059, https://doi.org/10.1016/j.desal.2022.116059.

[9] A. Mollahosseini, A. Abdelrasoul, Recent advances in thin film composites membranes for brackish groundwater treatment with critical focus on Saskatchewan water sources, J. Environ. Sci. 81 (2019) 181–194, https://doi.org/10.1016/j.jes.2019.01.014.

[10] F. Yang, H. Sadam, Y. Zhang, J. Xia, X. Yang, J. Long, S. Li, L. Shao, A de novo sacrificial-MOF strategy to construct enhanced-flux nanofiltration membranes for efficient dye removal, Chem. Eng. Sci. 225 (2020), 115845, https://doi.org/10.1016/j.ces.2020.115845.

[11] X. Lu, M. Elimelech, Fabrication of desalination membranes by interfacial polymerization: history, current efforts, and future directions, Chem. Soc. Rev. 50 (2021) 6290–6307, https://doi.org/10.1039/d0cs00502a.

[12] C.Y. Zhu, C. Liu, J. Yang, B.B. Guo, H.-N. Li, Z.K. Xu, Polyamide nanofilms with linearly-tunable thickness for high performance nanofiltration, J. Membr. Sci. 627 (2021), 119142, https://doi.org/10.1016/j.memsci.2021.119142.

[13] A. Li, Q. Rao, F. Liang, L. Song, X. Zhan, F. Chen, J. Chen, Q. Zhang, Polyhydroxy group functionalized zwitterion for a polyamide nanofiltration membrane with high water permeation and antifouling performance, ACS Appl. Polym. Mater. 2 (2020) 3850–3858, https://doi.org/10.1021/acsapm.0c00551.

[14] Z. Tan, S. Chen, X. Peng, L. Zhang, C. Gao, Polyamide membranes with nanoscale turing structures for water purification, Science 360 (2018) 518–521, https://doi.org/10.1126/science.aar6308.

[15] A. Tang, C. Fang, W. Feng, J. Lu, J. Li, L. Zhu, Engineering novel thin-film composite membranes with crater-like surface morphology using rigidly-contorted monomer for high flux nanofiltration, Desalination 509 (2021), 115067, https://doi.org/10.1016/j.desal.2021.115067.

[16] S. Karan, Z. Jiang, A.G. Livingston, Sub-10 nm polyamide nanofilms with ultrafast solvent transport for molecular separation, Science 348 (2015) 1347–1351, https://doi.org/10.1126/science.aaa1313.

[17] H. Guo, Y. Deng, Z. Tao, Z. Yao, J. Wang, C. Lin, T. Zhang, B. Zhu, C.Y. Tang, Does hydrophilic polydopamine coating enhance membrane rejection of hydrophobic endocrine-disrupting compounds? Environ. Sci. Tech. Lett. 3 (2016) 332–338, https://doi.org/10.1021/acs.estlett.6b00263.

[18] Y. Hao, Q. Li, B. He, B. Liao, X. Li, M. Hu, Y. Ji, Z. Cui, M. Younas, J. Li, An ultrahighly permeable-selective nanofiltration membrane mediated by an in situ formed interlayer, J. Mater. Chem. A. 8 (2020) 5275–5283, https://doi.org/10.1039/C9TA12258C.

[19] Z. Yang, Z.W. Zhou, H. Guo, Z. Yao, X.H. Ma, X. Song, S.P. Feng, C.Y. Tang, Tannic acid/Fe^{3+} nanoscaffold for interfacial polymerization: toward enhanced nanofiltration performance, Environ. Sci. Technol. 52 (2018) 9341–9349, https://doi.org/10.1021/acs.est.8b02425.

[20] M.B. Wu, Y. Lv, H.C. Yang, L.F. Liu, X. Zhang, Z.K. Xu, Thin film composite membranes combining carbon nanotube intermediate layer and microfiltration support for high nanofiltration performances, J. Membr. Sci. 515 (2016) 238–244, https://doi.org/10.1016/j.memsci.2016.05.056.

[21] J.J. Wang, H.C. Yang, M.B. Wu, X. Zhang, Z.K. Xu, Nanofiltration membranes with cellulose nanocrystals as an interlayer for unprecedented performance, J. Mater. Chem. 5 (2017) 16289–16295, https://doi.org/10.1039/C7TA00501F.

[22] D. Xu, X. Zhu, X. Luo, Y. Guo, Y. Liu, L. Yang, X. Tang, G. Li, H. Liang, MXene nanosheet templated nanofiltration membranes toward ultrahigh water transport, Environ. Sci. Technol. 55 (2021) 1270–1278, https://doi.org/10.1021/acs.est.0c06835.

[23] J. Yuan, M. Wu, H. Wu, Y. Liu, X. You, R. Zhang, Y. Su, H. Yang, J. Shen, Z. Jiang, Covalent organic framework-modulated interfacial polymerization for ultrathin desalination membranes, J. Mater. Chem. 7 (2019) 25641–25649, https://doi.org/10.1039/c9ta08163a.

[24] J. Zhu, J. Hou, S. Yuan, Y. Zhao, Y. Li, R. Zhang, M. Tian, J. Li, J. Wang, B. Van der Bruggen, MOF-positioned polyamide membranes with a fishnet-like structure for elevated nanofiltration performance, J. Mater. Chem. 7 (2019) 16313–16322, https://doi.org/10.1039/C9TA02299F.

[25] M. Zhang, X. You, K. Xiao, Z. Yin, J. Yuan, J. Zhao, C. Yang, R. Zhang, H. Wu, Z. Jiang, Modulating interfacial polymerization with phytate as aqueous-phase additive for highly-permselective nanofiltration membranes, J. Membr. Sci. 657 (2022), 120673, https://doi.org/10.1016/j.memsci.2022.120673.

[26] Y.-X. Li, P. Li, Y.-Z. Wu, Z.-L. Xu, M.-L. Huang, Preparation and antifouling performance of thin inorganic ultrafiltration membrane assisted sol-gel method with different composition of dual additives, Ceram. Int. 47 (2021) 2180–2186, https://doi.org/10.1016/j.ceramint.2020.09.056.

[27] Y.H. Teow, A.W. Mohammad, New generation nanomaterials for water desalination: a review, Desalination 451 (2019) 2–17, https://doi.org/10.1016/j.desal.2017.11.041.

[28] Y. Li, X. You, Y. Li, J. Yuan, J. Shen, R. Zhang, H. Wu, Y. Su, Z. Jiang, Graphene quantum dot engineered ultrathin loose polyamide nanofilms for high-performance nanofiltration, J. Mater. Chem. 8 (2020) 23930–23938, https://doi.org/10.1039/D0TA09319J.

[29] B. Wu, N. Wang, J.H. Lei, Y. Shen, Q.F. An, Intensification of mass transfer for zwitterionic amine monomers in interfacial polymerization to fabricate monovalent salt/antibiotics separation membrane, J. Membr. Sci. 643 (2022), 120050, https://doi.org/10.1016/j.memsci.2021.120050.

[30] M. Wang, M. Li, Z. Fei, J. Li, Z. Ren, Y. Hou, Synergistic regulation of macrocyclic polyamine-based polyamide nanofiltration membranes by the interlayer and surfactant for divalent ions rejection and mono-/di-ions sieving, Desalination 544 (2022), 116131, https://doi.org/10.1016/j.desal.2022.116131.

[31] Ö.V. Rúnarsson, J. Artacho, K. Wärnmark, The 125th Anniversary of the Tröger's base molecule: synthesis and applications of Tröger's base analogues, Eur. J. Org. Chem. 2012 (2012) 7015–7041, https://doi.org/10.1002/ejoc.201201249.

[32] B. Dolenský, M. Havlík, V. Král, Oligo Tröger's bases-new molecular scaffolds, Chem. Soc. Rev. 41 (2012) 3839–3858, https://doi.org/10.1039/c2cs15307f.

[33] L. Trupp, A.C. Bruttomesso, B.C. Barja, Simple dissymmetrical and asymmetrical Tröger's bases: photophysical and structural characterization, New J. Chem. 44 (2020) 10973–10981, https://doi.org/10.1039/D0NJ01988G.

[34] Z.G. Wang, X. Liu, D. Wang, J. Jin, Tröger's base-based copolymers with intrinsic microporosity for CO_2 separation and effect of Tröger's base on separation performance, Polym. Chem. 5 (2014) 2793–2800, https://doi.org/10.1039/c3py01608k.

[35] V. Talianová, T. Bříza, L. Krčová, B. Dolenský, J. Králová, P. Martásek, V. Král, M. Havlík, Coumarin Tröger's base derivatives with cyanine substitution as selective and sensitive fluorescent lysosomal probes, Bioorg. Chem. 94 (2020), 103447, https://doi.org/10.1016/j.bioorg.2019.103447.

[36] A. Lauber, B. Zelenay, J. Cvengroš, Asymmetric synthesis of N-stereogenic molecules: diastereoselective double aza-Michael reaction, Chem. Commun. 50 (2014) 1195–1197, https://doi.org/10.1039/c3cc48486f.

[37] F.A. Carey, Richard J. Sundberg, Advanced organic chemistry, in: Part A: Structure and Mechanisms, fifth ed., Springer, 2007.

[38] J. Tian, H. Chang, S. Gao, Y. Zong, B. Van der Bruggen, R. Zhang, Direct generation of an ultrathin (8.5 nm) polyamide film with ultrahigh water permeance via in-situ interfacial polymerization on commercial substrate membrane, J. Membr. Sci. 634 (2021), 119450, https://doi.org/10.1016/j.memsci.2021.119450.

[39] C. Jiang, L. Zhang, P. Li, H. Sun, Y. Hou, Q.J. Niu, Ultrathin film composite membranes fabricated by novel in situ free interfacial polymerization for desalination, ACS Appl. Mater. Interfaces 12 (2020) 25304–25315, https://doi.org/10.1021/acsami.0c05166.

[40] W.R. Bowen, J.S. Welfoot, Modelling of membrane nanofiltration-pore size distribution effects, Chem. Eng. Sci. 57 (2002) 1393–1407, https://doi.org/10.1016/S0009-2509(01)00412-2.

[41] E. Vellenga, G. Trägårdh, Nanofiltration of combined salt and sugar solutions: coupling between retentions, Desalination 120 (1998) 211–220, https://doi.org/10.1016/S0011-9164(98)00219-7.

[42] C. Jiang, L. Tian, Y. Hou, Q.J. Niu, Nanofiltration membranes with enhanced microporosity and inner-pore interconnectivity for water treatment: excellent balance between permeability and selectivity, J. Membr. Sci. 586 (2019) 192–201, https://doi.org/10.1016/j.memsci.2019.05.075.

[43] Z.M. Zhan, Z.L. Xu, K.K. Zhu, Y.-J. Tang, How to understand the effects of heat curing conditions on the morphology and performance of polypiperazine-amide NF membrane, J. Membr. Sci. 597 (2020), 117640, https://doi.org/10.1016/j.memsci.2019.117640.

[44] V. Freger, G.Z. Ramon, Polyamide desalination membranes: formation, structure, and properties, Prog. Polym. Sci. 122 (2021), 101451, https://doi.org/10.1016/j.progpolymsci.2021.101451.